TECHNICAL RESEARCH REPORT

SYSTEMS RESEARCH CENTER

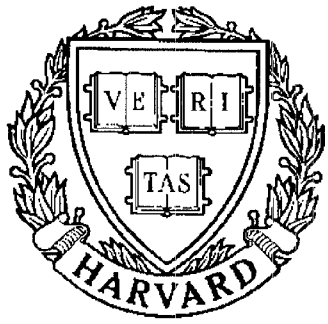

Supported by the National Science Foundation Engineering Research Center Program (NSFD CD 8803012), the University of Maryland, Harvard University, and Industry

Dynamic Simulation of Tendon-Driven Manipulators

by J.-J. Lee and L.-W. Tsai

TR 91-53

Dynamic Simulation Of Tendon-Driven Manipulators

Jyh-Jone Lee
Graduate Research Assistant

Lung-Wen Tsai
Professor

Mechanical Engineering Department
and
Systems Research Center
University of Maryland
College Park, MD 20742

ABSTRACT

This paper investigates some dynamic characteristics of tendon-driven manipulators. The dynamic equations including the effect of rotor inertia for a class of $n \times (n+1)$ tendon-driven manipulators are formulated. A control algorithm based on the computed torqued method is developed. Then, the implementation of such control algorithm is demonstrated in the simulation of a three-DOF tendon-driven manipulator. Through the simulation, several dynamic characteristics of the system are identified. In particular, it is shown that rotor inertia can have significant effect on the system dynamics and that pretension can play an important role on the stability of the system. It is also shown that among the five non-isomorphic kinematic structures of three-DOF manipulators, the one which satisfies the isotropic transmission and least maximum tendon force conditions also requires smallest tendon force in the dynamic simulations.

1. Introduction

Tendons have been used as transmission elements in the design of robot manipulators (Salisbury, 1982; Jacobsen, et al., 1984) . In robots, tendon transmission permits actuators to be installed remotely from the joints they drive and, therefore, reduces the size and inertia of the manipulating system. In addition, pretensioned tendons have no backlash. These merits have made tendon transmission more eminent in the design of manipulators, especially, in dextrous hand design where the requirements of small size and light weight are crucial. Therefore, a fundamental understanding of tendon transmission is important for better design of such manipulators.

This paper addresses some aspects of the dynamic characteristics and control associated with tendon-driven manipulators. Although the control problem of tendon-driven manipulators has been investigated by a few researchers (Salisbury,

1984; Venkataraman and Djaferis, 1987; and Jacobsen, et al. 1989), the problem is still relatively unexplored, and it can be further complicated by friction, compliance, and the coupling of displacements and forces in tendons. In general, the control problem consists of: 1) kinematic and dynamic modelling of the system, and 2) design of control strategies to achieve desired system performance. The objective of this paper is to study the dynamic characteristics including the effect of rotor inertia, and to suggest appropriate control strategies for tendon-driven manipulators.

First, a dynamic model for tendon-driven manipulators will be established under the assumption that friction and compliance effects in tendons are negligible. Following the derivation, a control algorithm based on computed torque method will be described. This algorithm assumes that feedback signals from sensors at each joint can be used to compute torques required for the motors. Then, based on the developed model, simulation results for the realization of dynamic characteristics of a sample tendon-driven manipulator will be presented.

In what follows, we shall neglect the inertia of pulleys used for power transmission, and we shall limit ourselves in those articulated manipulators which become open-loop chains after the pulleys and cables are removed.

2. Dynamic Modelling

We now proceed to the dynamic modelling of a tendon-driven manipulator. First, a general methodology will be developed and then, a three-DOF system will be used to demonstrate the concept. The dynamics of a tendon-driven manipulator can be divided into three parts: 1) dynamics of the open-loop chain, 2) kinematic relationship between the joint space and tendon space, and 3) rotor dynamics.

Dynamics of the Open – Loop Chain

The generalized dynamic equations of motion for an open-loop chain can be derived by the Lagrangian Mechanics. The equations of motion without gravity

term for a n-DOF manipulator can be expressed as (Paul, 1981):

$$M(\theta)\ \underline{\ddot{\Theta}} + \ \underline{h}(\theta, \dot{\theta}) = \ \underline{\tau} \tag{1}$$

where $M(\theta)$ is an $n \times n$ inertia matrix, $\underline{\Theta}$ an $n \times 1$ vector representing the joint angles θ, $\underline{h}(\theta, \dot{\theta})$ an $n \times 1$ vector representing the Centrifugal and Coriolis terms, and $\underline{\tau}$ an $n \times 1$ vector representing the resultant joint torques in the open-loop chain.

Kinematic Relationship Between Joint Space and Tendon Space

The force and displacement transformation between the joint space and tendon space were previously derived by Tsai and Lee (1989). In the force transformation, the resultant torques, $\underline{\tau} = (\tau_n, \tau_{n-1}, \cdots, \tau_2, \tau_1)^T$, about the joint axes in the equivalent open-loop chain can be related to tendon forces, $\underline{F} = (f_1, f_2, \cdots, f_n, f_{n+1})^T$, by the equation

$$\underline{\tau} = R^T B^T \underline{F} \tag{2.a}$$

where it is assumed that all pulleys pivoted about one joint axis are of the same radii, and the matrix B^T whose elements consists of -1, 0, and +1 is an $n \times (n+1)$ matrix, and the matrix R^T whose non-zero elements are the radii of the pulleys is an $n \times n$ diagonal matrix.

As to the displacement transformation, linear displacement of the tendons, $\underline{S} = (s_1, s_2, \cdots, s_n, s_{n+1})^T$, can be related to the joint angles, $\underline{\Theta} = (\theta_n, \theta_{n-1}, \cdots, \theta_2, \theta_1)^T$, by the equation

$$\underline{S} = BR\underline{\Theta} \tag{2.b}$$

In the above notations, the joints have been numbered in a sequential manner starting from the base.

Rotor Dynamics

The motor rotor dynamics can be approximated by a second-order system. Consider the ith tendon spooling system as shown in Fig. 1. If the ith tendon

is wound around the ith pulley of radius r_{m_i}, and the pulley is coupled to a gear reducer having a gear ratio of $n_i = r_g/r_p$ $(n_i \geq 1)$, then the torque developed by the ith motor is equal to the sum of the inertia torque, friction torque, and the torque reflected at the motor shaft due to tension in the tendon. Specifically, the equation can be written as

$$j_{m_i}\ddot{\theta}_{m_i} + c_{m_i}\dot{\theta}_{m_i} + \frac{r_{m_i}}{n_i} f_i = \xi_i \qquad (3.a)$$

where j_{m_i}, c_{m_i}, θ_{m_i}, f_i, and ξ_i denote the rotor inertia, viscous-friction coefficient, rotor angular displacement, tension in the ith tendon, and torque developed by the ith motor, respectively.

Since there are $(n+1)$ motors for an n-DOF tendon-driven manipulator, Eq.(3.a) can be written $(n+1)$ times, once for each motor. These $(n+1)$ dynamic equations can be compiled into a matrix form as shown below:

$$J_m\underline{\ddot{\Theta}}_m + C_m\underline{\dot{\Theta}}_m + R_m\underline{F} = \underline{\xi} \qquad (3.b)$$

where J_m, C_m, and R_m are $(n+1)\times(n+1)$ diagonal matrices whose diagonal elements are j_{m_i}, c_{m_i}, and $\frac{r_{m_i}}{n_i}$, respectively; $\underline{F}$ is an $(n+1)\times 1$ vector representing tensions in the tendons; and $\underline{\Theta}_m$ and $\underline{\xi}$ are $(n+1)\times 1$ vectors whose elements are the rotor angular displacements and motor torques, respectively.

Overall System Dynamics

The rotor angular displacements can be related to the manipulator joint angles by $R_m\underline{\Theta}_m = BR\underline{\Theta}$. Substituting this relationship into Eq. (3.b), one can solve tendon forces in terms of motor torques and joint angles as:

$$\underline{F} = {R_m}^{-1}[\underline{\xi} - J_m{R_m}^{-1}BR\underline{\ddot{\Theta}} - C_m{R_m}^{-1}BR\underline{\dot{\Theta}}] \qquad (4)$$

Substituting Eqs. (4) and (2.a) into (1), yields

$$(M + \tilde{M})\underline{\ddot{\Theta}} + \tilde{C}_m\underline{\dot{\Theta}} + \underline{h}(\theta,\dot{\theta}) = R^T B^T {R_m}^{-1}\underline{\xi} \qquad (5)$$

where $\tilde{M} = R^T B^T {R_m}^{-1} J_m {R_m}^{-1} BR$ denotes the inertias of the rotors reflected at the joints, and $\tilde{C}_m = R^T B^T {R_m}^{-1} C_m {R_m}^{-1} BR$ denotes the viscous damping of the rotors reflected at the joints.

Equation (5) completely describes the dynamics of a class of $n \times (n+1)$ tendon-driven manipulators. Note that the term $R^T B^T {R_m}^{-1} \underline{\xi}$ on the right-hand-side of Eq. (5) does not represent the resultant joint torques. The term $\tilde{M}$ gives the effect of rotor inertia and the term $\tilde{C}_m$ gives the effect of damping to the dynamics of the system. It should be also noted that tendon tensions given by Eq.(4) must be positive at all times for the dynamic model to be valid. This will be described in more detail in Section 3.

3. Computed Torque Controller

The purpose of a controller is to servo the motors so that the end-effector will trace a desired path. In this work, the "computed torque" technique will be implemented for controlling the manipulator. The technique assumes that one can accurately compute the configuration dependent variables, $M(\theta)$ and $\underline{h}(\theta, \dot{\theta})$, in the equations of motion to minimize their nonlinear effects. Using a proportional plus a derivative feedback, the proposed control law consists of the following two terms:
(i) Compensation of the Centrifugal/Coriolis force and the viscous friction terms:

$$\tilde{C}_m \dot{\underline{\Theta}} + \underline{h}(\theta, \dot{\theta}) \tag{6}$$

(ii) Proportional and derivative feedback terms:

$$(M + \tilde{M})[\ddot{\underline{\Theta}}_d + K_v \dot{\underline{e}} + K_p \underline{e}] \tag{7}$$

where K_v and K_p are respectively $n \times n$ derivative and positional feedback gain matrices, $\underline{\Theta}_d$ is the desired joint angular displacement vector, and $\underline{e} \equiv \underline{\Theta}_d - \underline{\Theta}$ is the error vector.

If the structure of the control law contains the above two terms, then the tracking error $\underline{e}(t)$ will approach zero asymptotically. This can be explained as follows. Let the computed torques $\underline{\tau}_{cm}$ be related to the motor torques by

$$\underline{\tau}_{cm} = R^T B^T {R_m}^{-1} \underline{\xi} \tag{8.a}$$

and let the value of $\underline{\tau}_{cm}$ be computed from joint feedback signals as

$$\underline{\tau}_{cm} = (M + \tilde{M})[\underline{\ddot{\Theta}}_d + K_v \underline{\dot{e}} + K_p \underline{e}] + \tilde{C}_m \underline{\dot{\Theta}} + \underline{h}(\theta, \dot{\theta}) \tag{8.b}$$

Then, substituting Eqs.(8.a) and (8.b) into (5), yields

$$\begin{aligned} &(M + \tilde{M})\underline{\ddot{\Theta}} + \tilde{C}_m \underline{\dot{\Theta}} + \underline{h}(\theta, \dot{\theta}) \\ &= \underline{\tau}_{cm} \\ &= (M + \tilde{M})[\underline{\ddot{\Theta}}_d + K_v \underline{\dot{e}} + K_p \underline{e}] + \tilde{C}_m \underline{\dot{\Theta}} + \underline{h}(\theta, \dot{\theta}) \end{aligned} \tag{9.a}$$

After some simplification, Eq. (9.a) becomes

$$(M + \tilde{M})(\underline{\ddot{e}} + K_v \underline{\dot{e}} + K_p \underline{e}) = 0 \tag{9.b}$$

Since $(M + \tilde{M})$ is always nonsingular, one can choose K_v and K_p appropriately so that the characteristic roots of Eq. (9.b) have proper negative real parts and the tracking error $\underline{e}(t)$ approaches zero asymptotically.

Since the vector spaces of $\underline{\tau}_{cm}$ and $\underline{\xi}$ do not have the same dimension, the mapping between these two spaces is not one to one. In this study, the pseudo-inverse method will be used to convert the computed torque $\underline{\tau}_{cm}$ to the motor torque $\underline{\xi}$. The solution of $\underline{\xi}$ to Eq. (8.a) can be expressed as:

$$\underline{\xi} = (R^T B^T {R_m}^{-1})^+ \underline{\tau}_{cm} + \lambda \underline{\xi}_h \tag{10}$$

where $(\#)^+ = \{(\#)^T[(\#)(\#)^T]^{-1}\}$ represents the pseudo-inverse of $(\#)$ (Strang 1980), $\underline{\xi}_h$ lies in the null space of structure matrix $(R^T B^T {R_m}^{-1})$, and λ is an

arbitrary constant. By adjusting λ, motor torques can be adjusted to assure positive tension in tendons.

4. Implementation and Simulation Results

In this section the simulation of a three-DOF tendon-driven manipulator using the control algorithm developed in Sections 2 and 3 will be presented. Figure 2 shows five nonisomorphic, three-DOF kinematic structures developed in Lee and Tsai (1991(a)). The kinematic structure shown in Fig. 2(d) which satisfies isotropic transmission and least maximum tendon force conditions (Lee and Tsai, 1991(b); and Lee, 1991) will be used for illustration. Figure 3 shows the control block diagram for the system. Detailed dimensions of the manipulator used for the simulation are given in the Appendix.

Controller Design

The controller is designed according to Eq. (8.b). Figure 4 shows the detailed diagram of the controller shown in Fig. 3, where k_{p_i}, k_{v_i}, and m_{ij} are the elements of matrices K_p, K_v, and $(M + \tilde{M})$, respectively.

As mentioned in Section 2, it is necessary to keep tendon forces positive at all times in order for the dynamic simulation to be valid. The following heuristic has been implemented to assure positive tendon forces. In view of Eq. 4, to compensate for the uncertainty due to rotor inertia and viscous friction torques, motor torques are first computed by the pseudo-inverse method as shown by Eq. (10) so that the smallest motor torque is equal to zero. Then, maximum desired rotor acceleration and velocity, $\underline{\ddot{\Theta}}_m$ and $\underline{\dot{\Theta}}_m$, are used to estimate additional motor torques, $J_m(\ddot{\theta}_m)_{max}$ and $C_m(\dot{\theta}_m)_{max}$, needed for pretensioning the tendons.

Feedback Gains Design

The performance of a nonlinear system can be realized or compared if uniform criteria are used for the design of feedback system. That is, the gain matrices are

chosen to satisfy a specified output response criterion. To this end, the influence of feedback gains K_p and K_v on the positional response of the system has been investigated. Figure 5 shows the response of joint angle 3 to the simultaneous execution of step inputs to all the three joints for various damping ratios. The initial conditions for the simulations are $\theta_i = 0$ and $\dot{\theta}_i = 0$, (i=1,2,3), and the step function for each joint is applied at t=0.1 seconds with a step value of 0.2618 radians. Three sets of gain values are chosen for comparison, they are (K_p, K_v)=(225, 23), (225, 30), and (225, 35), respectively. It can be seen from Fig. 5 that the system is underdamped for the value of (K_p, K_v)=(225, 23); overdamped for the value of (225, 35); and critically damped for the value of (225, 30).

Since critical damping yields better system response, in what follows the gain matrices will be chosen such that the system is always critically damped, i.e.,

$$k_{v_i} = 2\sqrt{k_{p_i}}, \qquad i = 1, 2, 3 \tag{11}$$

In practice, one method for improving the response time is to increase the gains k_{p_i} and k_{v_i}. Increasing the gains also increases torque requirement on motors. However, it can result in an unstable situation. Figure 6 shows the response of the system to simultaneous step inputs of three joint angles for two different gain values. Both gains are chosen to satisfy the critically damped condition. It can be seen that the higher the gains are, the stiffer the system is. The demand of motor torques for these two gain values are plotted in Figs. 7(a) and 7(b), respectively. The maximum torque requirement is 7.76 $\times 10^4$ dyne-cm for the gain value of (225, 30) and 13.4 $\times 10^4$ dyne-cm for the gain value of (400, 40). To achieve high system response and stability, the gain value (225, 30) which demands about one third of the available motor torque will be used for the following studies. Note that a biased motor torque of 2045 dyne-cm has been added to all motors in order to obtain proper pretension of the tendons. The angular velocity and acceleration responses

of the motors are shown in Figs. 8 and 9, respectively. Note that the negative velocities of motors 1, 2, and 3 shown in Fig. 8 denote that the motors are under "back driving" condition, i.e., the direction of rotation is in the opposite direction of the motor torque applied.

Rotor Inertia and Viscous Friction Effects on Tendon Force

Figures 10 and 11 show the response of tendon forces for two different gains. In Fig. 10, the gain is (225, 30) and the lowest tendon tension occurs at the point B where the force magnitude is 1.67×10^4 dyne (45.5 % below the pretensioning force). On the other hand, in Fig. 11, the gain is (400, 40) and the point B has dropped to a value of 1.22×10^4 dyne (60.2 % below the pretensioning force). This is due to the effect of rotor inertia and viscous friction. Figures 12 and 13 respectively show motor torque and tendon force responses without considering the rotor inertias and viscous frictions. A comparison of the simulation results shown in Figs. 7 and 12 shows a significant difference on motor torques requirement, 7.64 $\times 10^4$ as compared to 4.3 $\times 10^4$ dyne-cm peak torque on motor 4. Comparing the tendon force curves shown in Figs. 10 and 13 also shows a significant difference in tensions. It can be seen that if pretensioning is not well managed, system modelling without considering motor inertia and viscous friction terms may cause slackness in tendons and result in an unstable situation. Hence, pretension may play an important role in the control of tendon-driven manipulators.

Maximum Motor Torque

This section compares the motor torque requirement among different kinematic structures. Given a kinematic structure, motor torque responses are simulated for various combinations of simultaneous step inputs. A step input can be applied either in the positive or negative direction of a joint. For a three-jointed manipulator, there are eight combinations of step inputs that can be applied to each kinematic

structure. Due to directional sensitivity in the manipulator, all combinations of the simultaneous step inputs are executed and the worst condition which requires maximum motor torque for each kinematic structure is recorded. For the kinematic structures shown in Figs. 2(a) to 2(d), the maximum motor torque occurs when the step inputs are applied in the $\theta_{1d} = \theta_{2d} = \theta_{3d} = 0.2618$ radians direction, while the maximum motor torque for the structure shown in Fig. 2(e) occurs when the step inputs are applied in the $\theta_{1d} = \theta_{3d} = 0.2618$ radians and $\theta_{2d} = -0.2618$ radians direction. Figures 7(a), and 14 through 17 show the simulation results. It can be observed that the kinematic structure as shown in Fig. 2(d) has the least maximum torque among all the kinematic structures.

5. Summary

The formulation of dynamic equations of motion and control algorithm for a general class of tendon-driven manipulators have been developed. The computed torque method has been employed to illustrate the principle of control algorithm and the pseudo-inverse technique has been used for transforming joint-torque signals to motor-torque signals. The integral of the control method in the simulation is demonstrated through a three-DOF tendon-driven manipulator. Several system characteristics have been investigated through the simulation.

We have shown that rotor inertia can have significant effect on the dynamics of the system even though the gear ratio is not very high. Hence, pretension can play an important role in the stability of the system. We have also shown that among five nonisomorphic kinematic structures of three-DOF tendon-driven manipulators, the one which satisfies isotropic transmission and least maximum tendon force conditions also requires smallest tendon force under dynamic conditions. It is hoped that this study will lead to a better understanding of tendon-driven manipulators.

Acknowledgement

This research has been supported in part by the Department of Energy, Grant No. DEFG05-88ER13977, and in part by the NSF's Engineering Research Centers Program, NSFD CDR 8803012. Such supports do not constitute an endorsement by the supporting agencies of the views expressed in the article.

References

Åström, K. J., 1985, *A SIMNON Tutorial,* Report of Dept. of Automatic Control, Lund Institute of Technology, Lund, Sweden.

Jacobsen, S. C., Wood, J. E., Knutti, D. F., and Biggers, K. B., 1984, "The Utah/MIT Dextrous Hand: Work in Progress," The Intl. Journal of Robotics Research, Vol. 3, No. 4, pp. 21-50.

Jacobsen, S. C., Ko, H., Iversen, E. K., and Davis, C. C., 1989, "Antagonistic Control of a Tendon Driven Manipulator," IEEE Proceedings of Intl. Conference on Robotics and Automation, pp. 1334-1339.

Lee, J. J., 1991, "Tendon-Driven Manipulators - Analysis, Synthesis, and Control," Ph.D. Dissertation, Dept. of Mechanical Engineering, the University of Maryland, College Park, MD.

Lee, J. J., and Tsai, L. W., 1991(a), "On the Structural Synthesis of Tendon-Driven Manipulators Having Pseudo-Triangular Matrix", The Intl. Journal of Robotics Research, Vol. 10, No. 3.

Lee, J. J., and Tsai, L. W., 1991(b), "Topological Analysis of Tendon-Driven Manipulators," to appear in the Proceedings of the 8th World Congress on the Theory of Machines and Mechanisms, Prague, Czechoslovakia.

Paul, R. P., 1981, *Robot Manipulator: Mathematics, Programming and Control,* MIT Press, Cambridge, MA.

Salisbury, J. K., 1982, "Kinematic and Force Analysis of Articulated Hands," Ph.D. Dissertation, Dept. of Mechanical Engineering, Stanford University, Stanford, CA.

Salisbury, J. K., 1984, "Design And Control of an Articulated Hand," Proceedings of the 1^{st} Intl. Symposium on Design and Synthesis, Tokyo, Japan.

Strang, G., 1980, *Linear Algebra and Its Applications*, Academic Press, Inc., Orlando, FL.

Tsai, L. W., and Lee, J. J., 1989, "Kinematic Analysis of Tendon-Driven Robotic Mechanisms Using Graph Theory," ASME J. of Mechanisms, Transmissions, and Automation in Design. Vol. 111, No.1, pp. 59-65.

Venkataraman, S. T., and Djaferis, T. E., 1987, "Multivariable Feedback Control of the JPL/Stanford Hand," IEEE Proceedings of Intl. Conference on Robotics and Automation, pp. 77-82.

Appendix: Dimensions of the open-loop chain

Figure A1 shows the configuration of the open-loop chain used in the simulation. It is assumed that the links are uniform and the mass center of each link is located in the middle of the link. The dynamic equations for the open-loop chain neglecting gravitational terms are given by:

$$\begin{aligned}
\tau_1 =&[m_1 {l_1}^2/3 + m_2({l_1}^2 + {l_2}^2 {c_2}^2/3 + l_1 l_2 c_2) + m_3(l_1 + l_2 c_2 + l_3 c_{23}/2)^2 + \\
&m_3 {l_3}^2 {c_{23}}^2/12]\ddot{\theta}_1 + h_1 \\
\tau_2 =&[m_2 {l_2}^2/3 + m_3({l_2}^2 + {l_3}^2/3 + l_2 l_3 c_3)]\ddot{\theta}_2 + [m_3 {l_3}^2/3 + m_3 l_2 l_3 c_3/2]\ddot{\theta}_3 + h_2 \\
\tau_3 =&[m_3({l_3}^2/3 + l_2 l_3 c_3/2)]\ddot{\theta}_2 + (m_3 {l_3}^2/3)\ddot{\theta}_3 + h_3 \qquad (A.1)
\end{aligned}$$

where

$$\begin{aligned}
h_1 =& - m_2\dot{\theta}_1\dot{\theta}_2[l_2(l_1 + l_2 c_2/2)s_2 + l_2^2 c_2 s_2/6] \\
&- m_3\dot{\theta}_1\dot{\theta}_3[(l_1 + l_2 c_2 + l_3 c_{23}/2)l_3 s_{23} + l_3^2 s_{23} c_{23}/6] \\
&- m_3\dot{\theta}_1\dot{\theta}_2[(l_1 + l_2 c_2 + l_3 c_{23}/2)(2l_2 s_2 + l_3 s_{23}) + l_3^2 c_{23} s_{23}/6]
\end{aligned}$$

$$\begin{aligned}
h_2 =&m_2(l_1 l_2 s_2/2 + {l_2}^2 c_2 s_2/3)\dot{\theta_1}^2 + m_3(l_1 + l_2 c_2 + l_3 c_{23}/2)(l_2 s_2 + l_3 s_{23})\dot{\theta}_1^2 \\
&+ m_3 {l_3}^2 \dot{\theta}_1^2 c_{23} s_{23}/12 - m_3 l_2 l_3(\dot{\theta}_2 + \dot{\theta}_3/2)s_3\dot{\theta}_3
\end{aligned}$$

$$h_3 = m_3 l_3 s_{23}\dot{\theta}_1^2[(l_1 + l_2 c_2 + l_3 c_{23}/2) + l_3 c_{23}/6]/2 + m_3 l_2 l_3 s_3 \dot{\theta}_2^2/2$$

and where $s_2 = \sin\theta_2$, $s_3 = \sin\theta_3$, $c_2 = \cos\theta_2$, $c_3 = \cos\theta_3$, $s_{23} = \sin(\theta_2 + \theta_3)$, and $c_{23} = \cos(\theta_2 + \theta_3)$.

The following numerical values are used for the simulation:
$m_1 = 90$ gm, $m_2 = m_3 = 100$ gm; $l_1 = 3$ cm, $l_2 = l_3 = 4$ cm; joint axis pulley radius: $r_1 = r_2 = r_3 = 0.8$ cm, spooler radius of the ith motor: $r_{m_i} = 0.8$ cm, gear ratio n_i=12, motor rotor inertia $j_{m_i} = 12.78$ dyne $-$ cm $-$ sec^2, viscous damping coefficient $c_{m_i} = 68.5$ dyne-cm-sec/rad, and maximum available motor torque=215400 dyne-cm, for all motors.

The simulation package SIMNON (Åström, 1985) is used to simulate the system. The plant is integrated under the continuous time system and the time step for integration is 0.005 sec.

Figure Captions

Fig. 1 Schematic of the motor-tendon spooling system

Fig. 2 Nonisomorphic kinematic structures having three-DOF

Fig. 3 Control block diagram of a three-DOF tendon-driven manipulator

Fig. 4 Design details of the controller shown in Fig. 3

Fig. 5 Joint angle response vs. various damping ratios

Fig. 6 The effect of feedback gain on system stiffness

Fig. 7(a) Motor torque response with K_p=225 and K_v=30, peak value= 7.64×10^4 dyne-cm

Fig. 7(b) Motor torque response with K_p=400 and K_v=40, peak value= 1.34×10^5 dyne-cm

Fig. 8 Motor rates with K_p=225 and K_v=30

Fig. 9 Motor accelerations with K_p=225 and K_v=30

Fig. 10 Tendon force response with K_p=225 and K_v=30, B= 1.67×10^4 dyne

Fig. 11 Tendon force response with K_p=400 and K_v=40, B=1.22×10^4 dyne

Fig. 12 Motor torque response without considering motor inertia and viscous friction (K_p=225 and K_v=30)

Fig. 13 Tendon force response without considering motor inertia and viscous friction (K_p=225 and K_v=30)

Fig. 14 Motor torque response for the structure shown in Fig. 2(a), peak value = 1.47×10^5 dyne-cm

Fig. 15 Motor torque response for the structure shown in Fig. 2(b), peak value = 2.19×10^5 dyne-cm

Fig. 16 Motor torque response for the structure shown in Fig. 2(c), peak value = 8.88×10^4 dyne-cm

Fig. 17 Motor torque response for the structure shown in Fig. 2(e), peak value = 1.11×10^5 dyne-cm

Fig. A1 Schematic of the open-loop chain

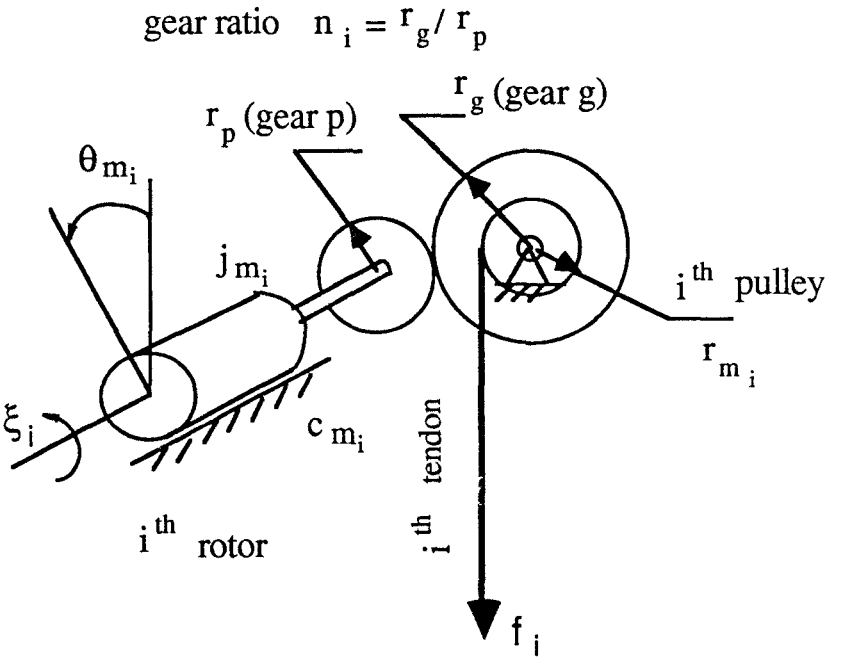

Fig. 1 Schematic of motor-tendon spooling system

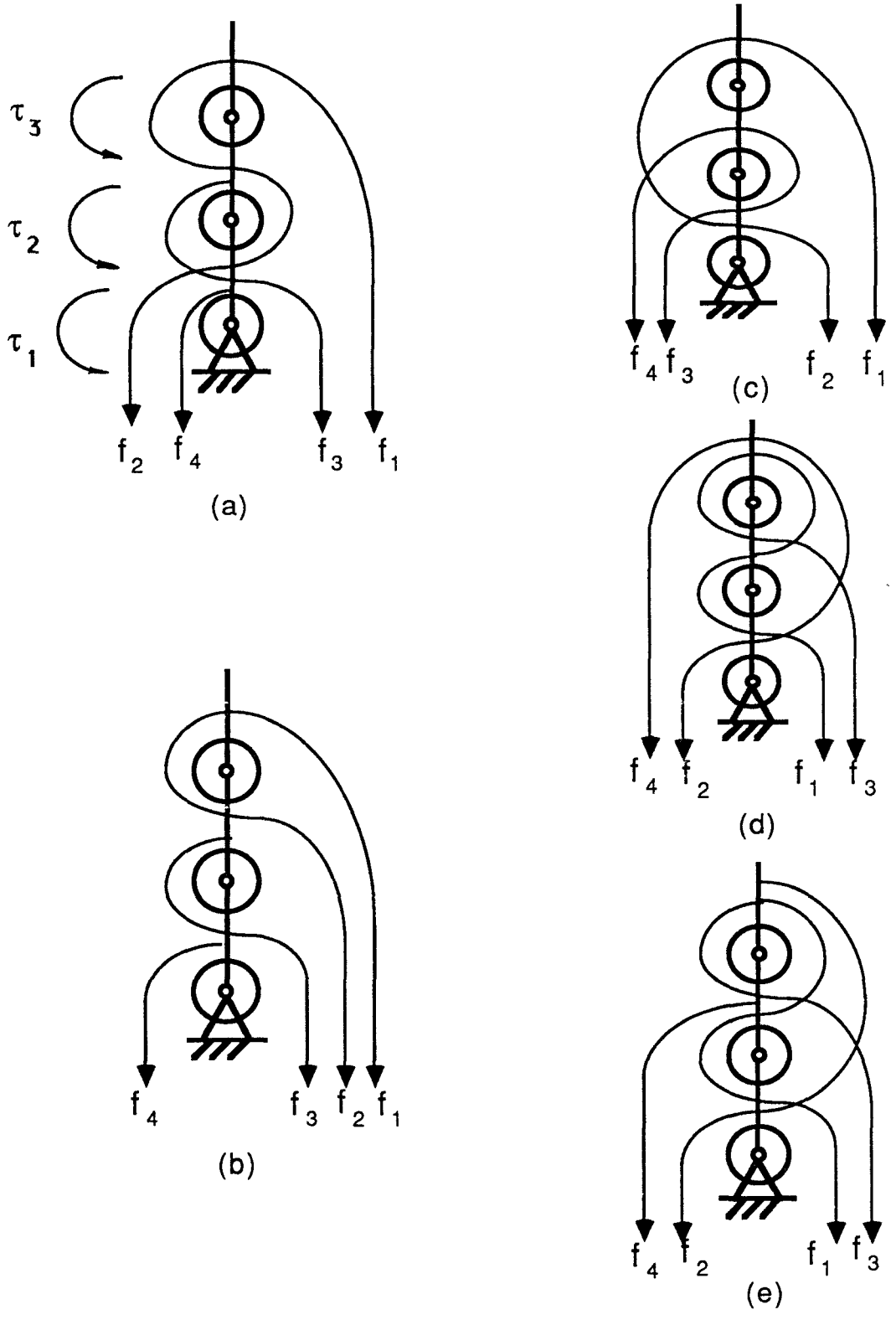

Fig. 2 Non-isomorphic kinematic structures having three-DOF

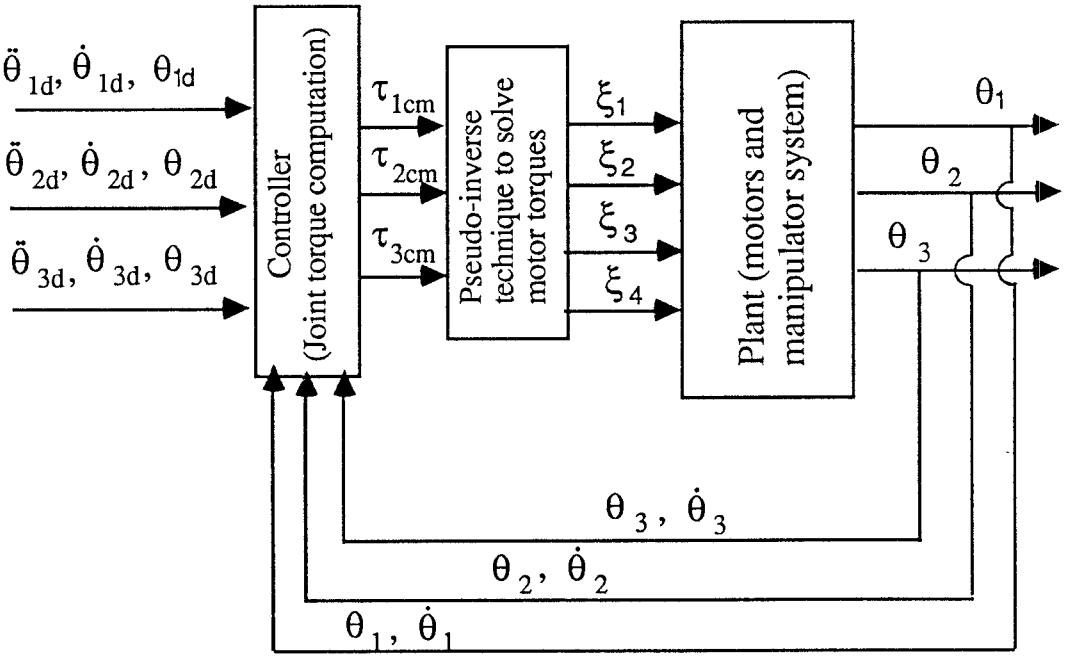

Fig. 3 Control block diagram of a three-DOF tendon-driven manipulator

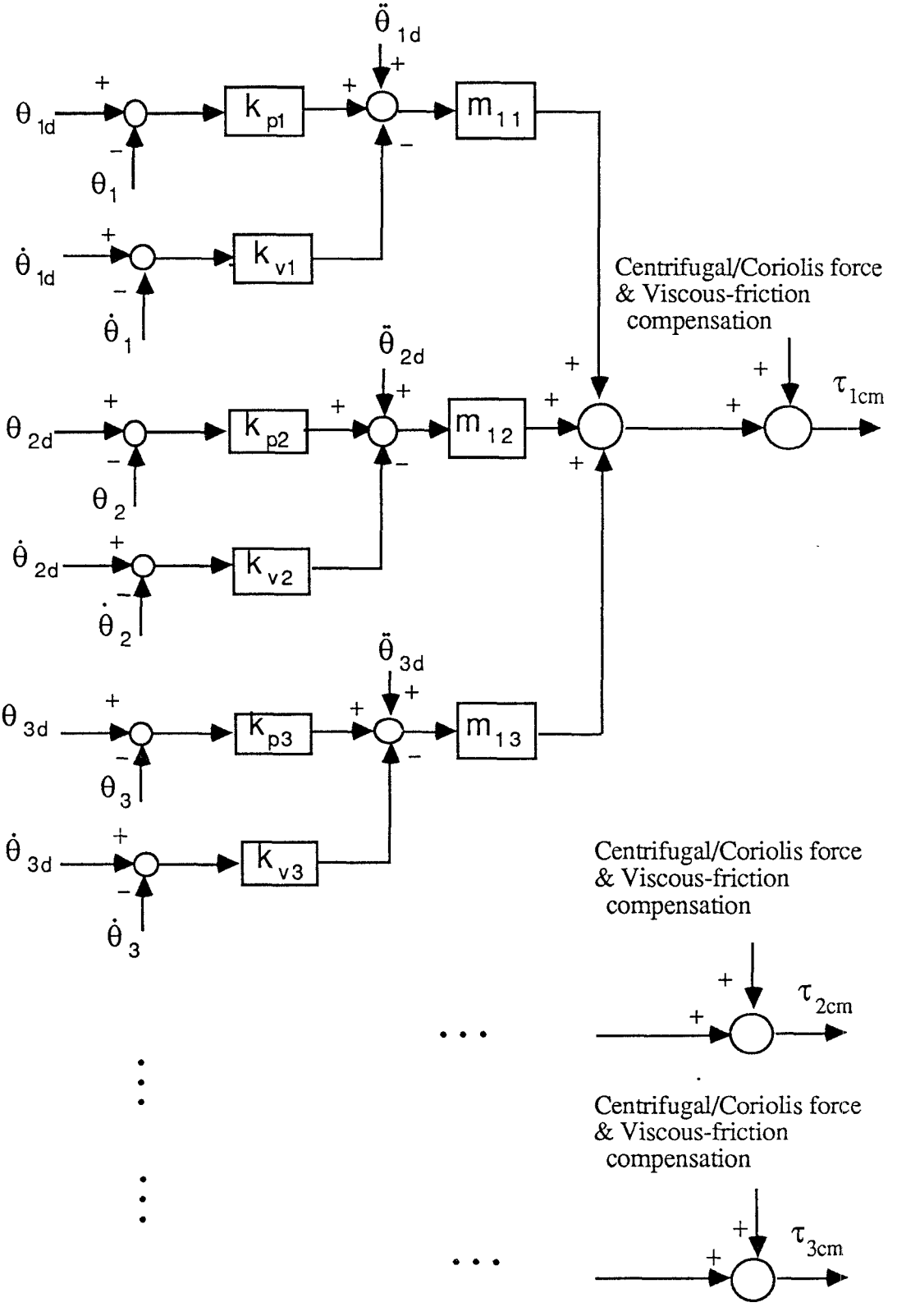

Fig. 4 Design details of the controller shown in Fig. 3

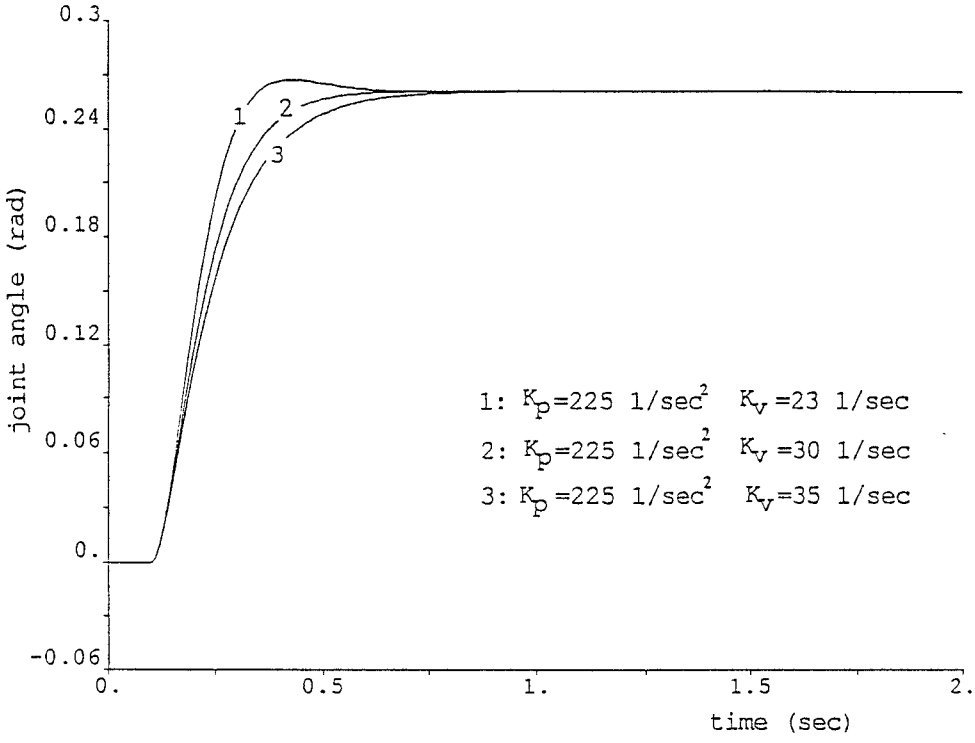

Fig. 5 Joint angle response vs. various damping ratios

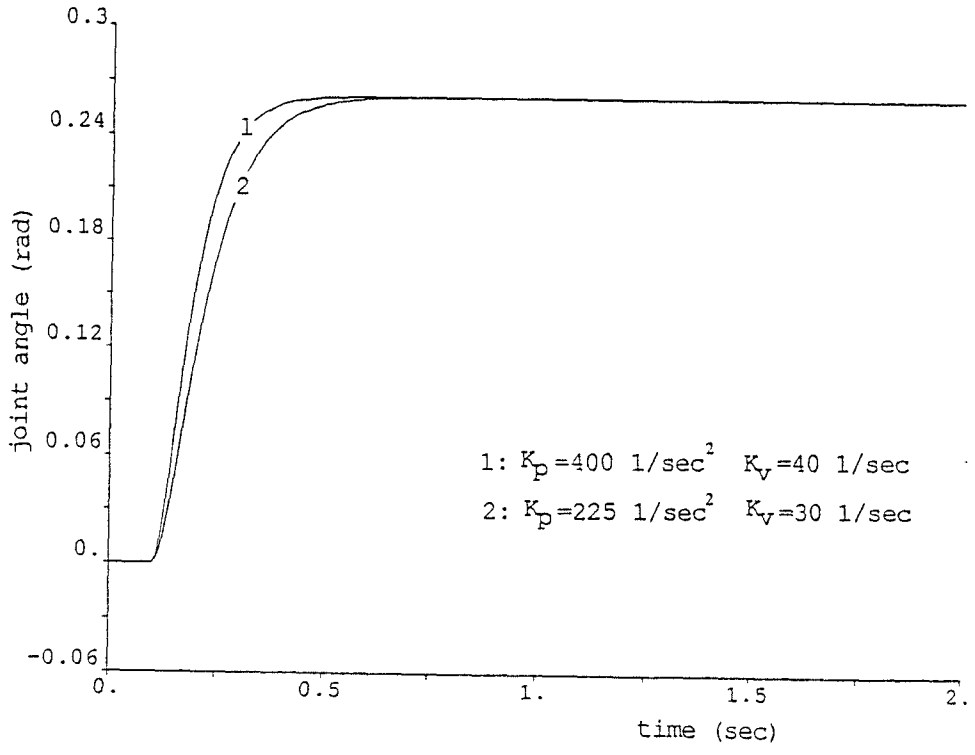

Fig. 6 The effect of feedback gain on system stiffness

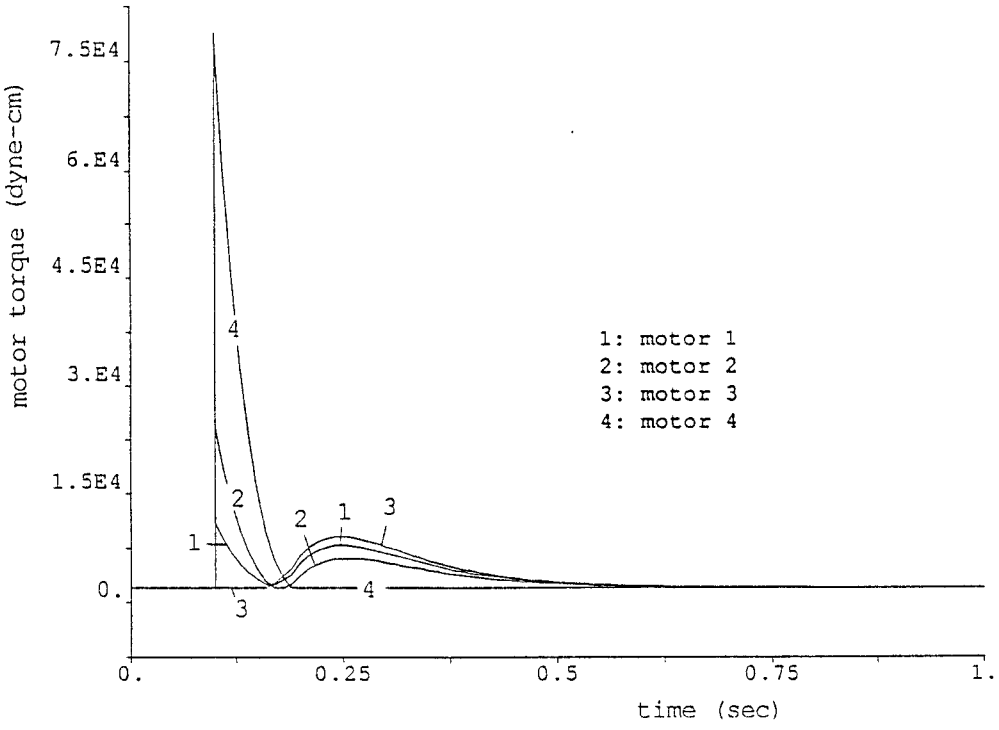

Fig. 7(a) Motor torque response with K_p=225 and K_v=30, peak value=7.64×10^4 dyne-cm

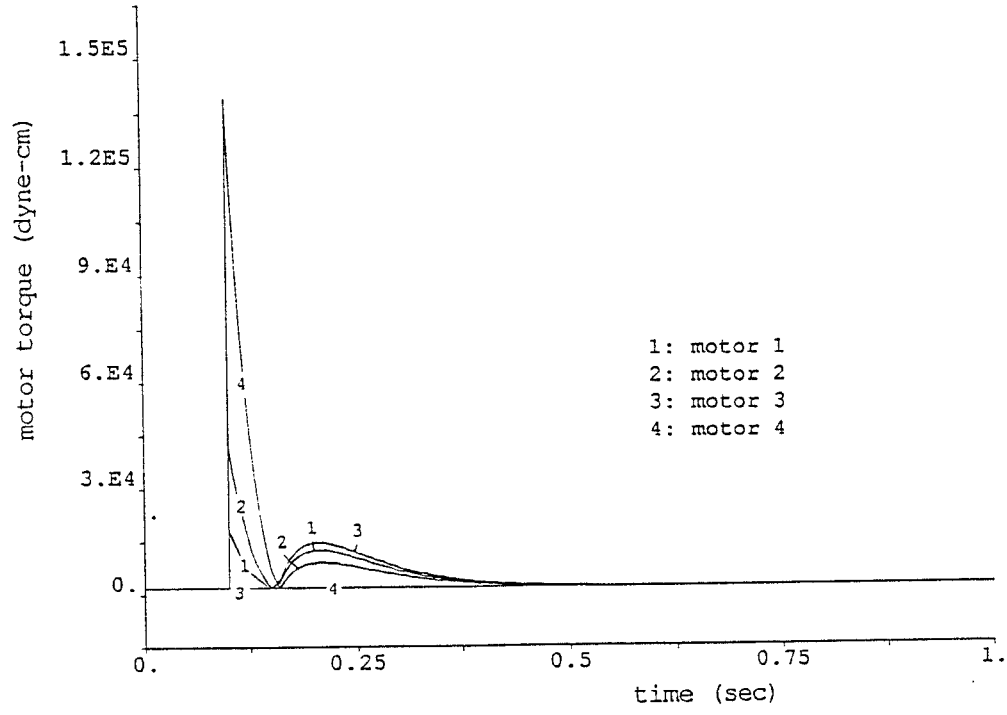

Fig. 7(b) Motor torque response with K_p=400 and K_v=40, peak value=1.34×10^5 dyne-cm

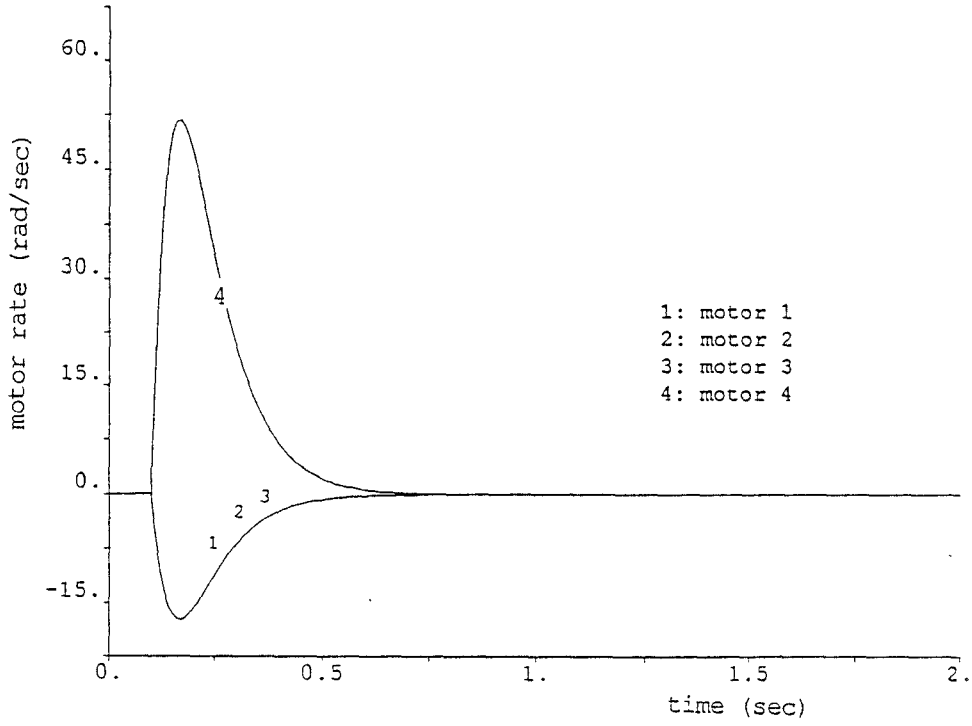

Fig. 8 Motor rates with K_p=225 and K_v=30

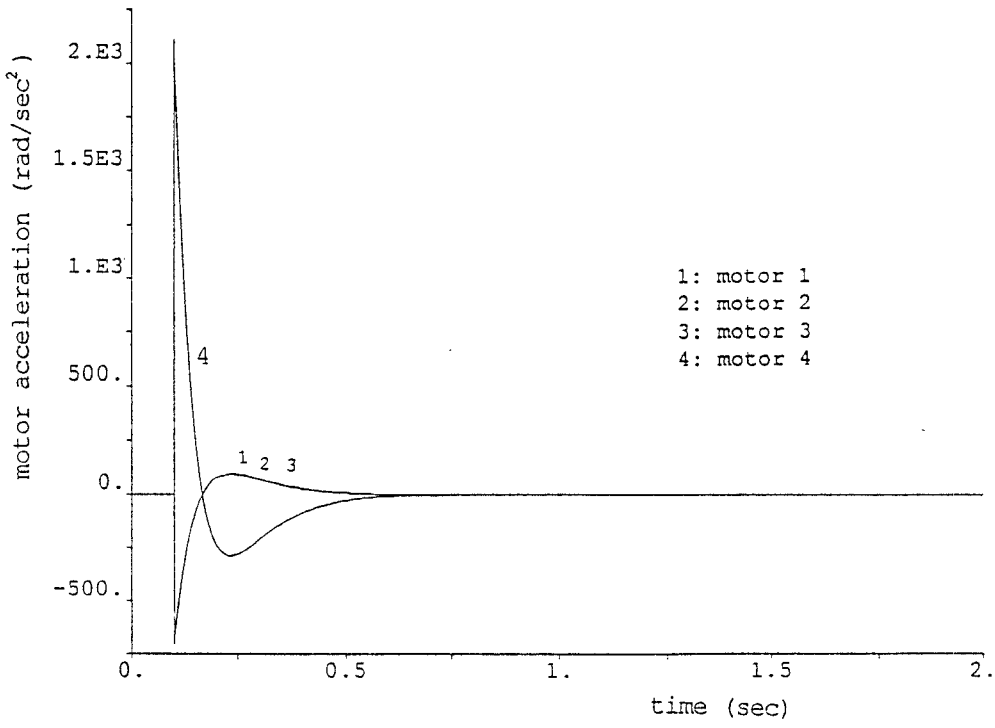

Fig. 9 Motor accelerations with K_p=225 and K_v=30

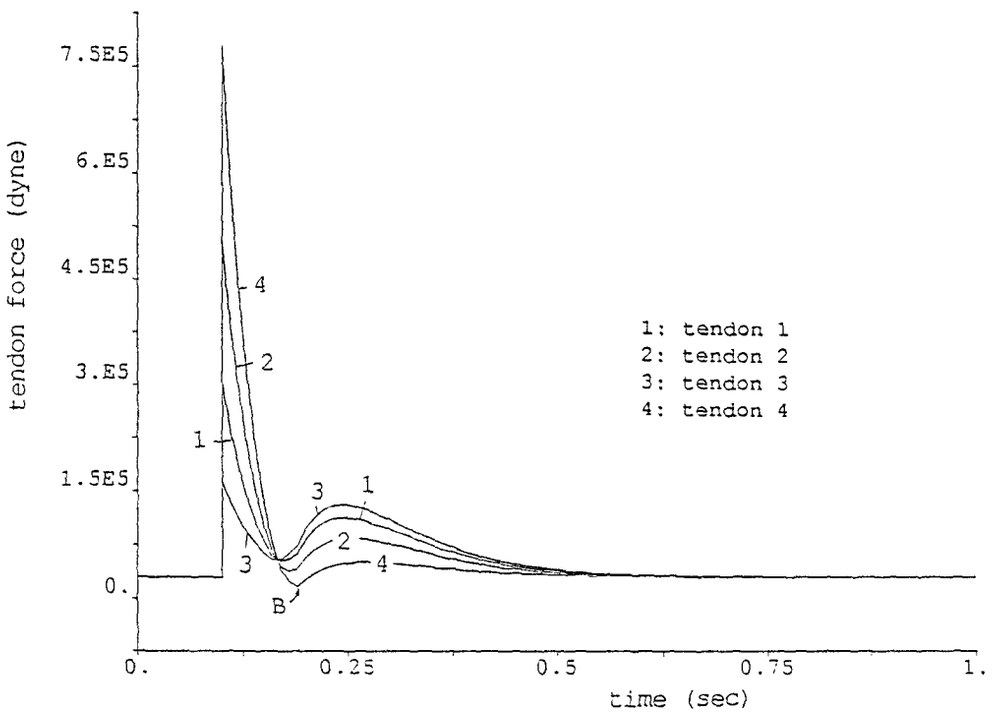

Fig. 10 Tendon force response with K_p=225 and K_v=30, B=1.67×10^4 dyne

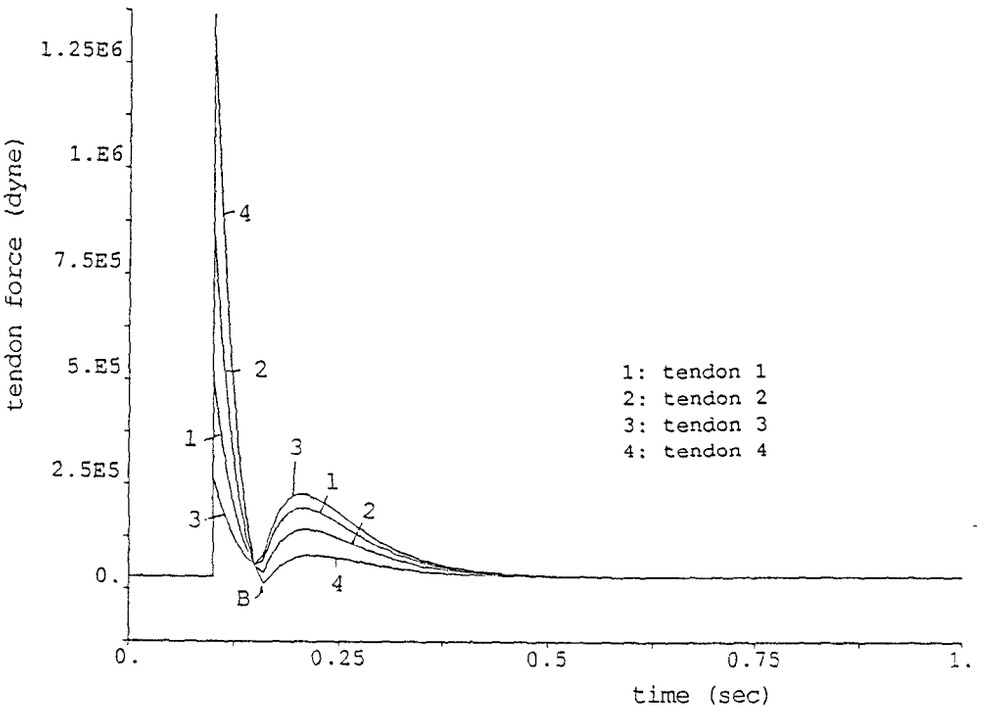

Fig. 11 Tendon force response with K_p=400 and K_v=40, B=1.22×10^4 dyne

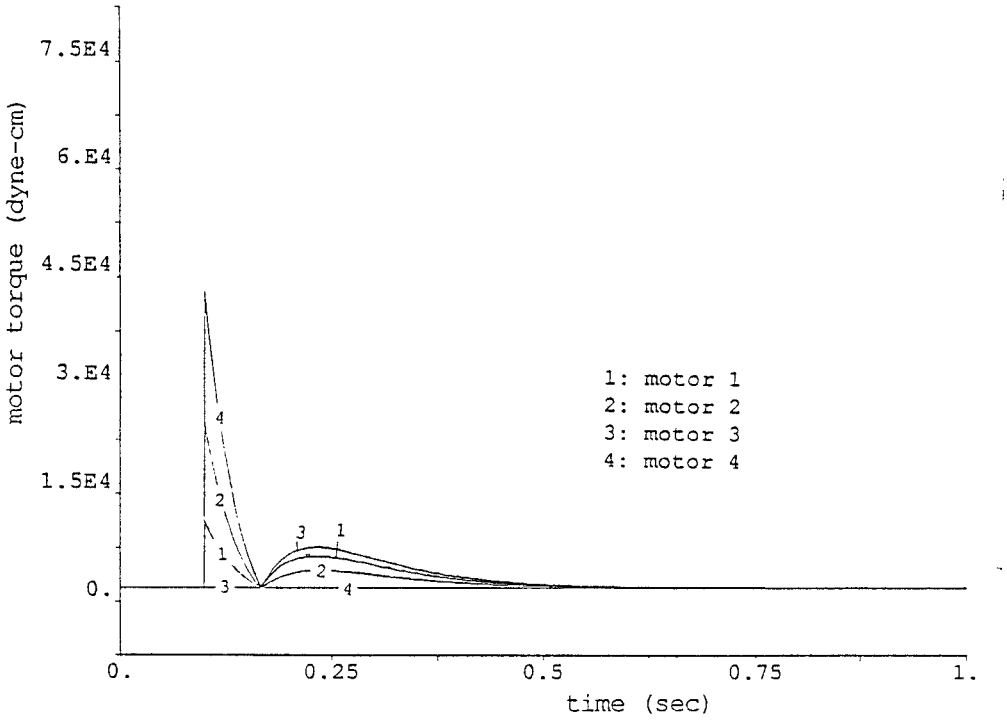

Fig. 12 Motor torque response without considering motor inertia and viscous friction (K_p=225 and K_v=30)

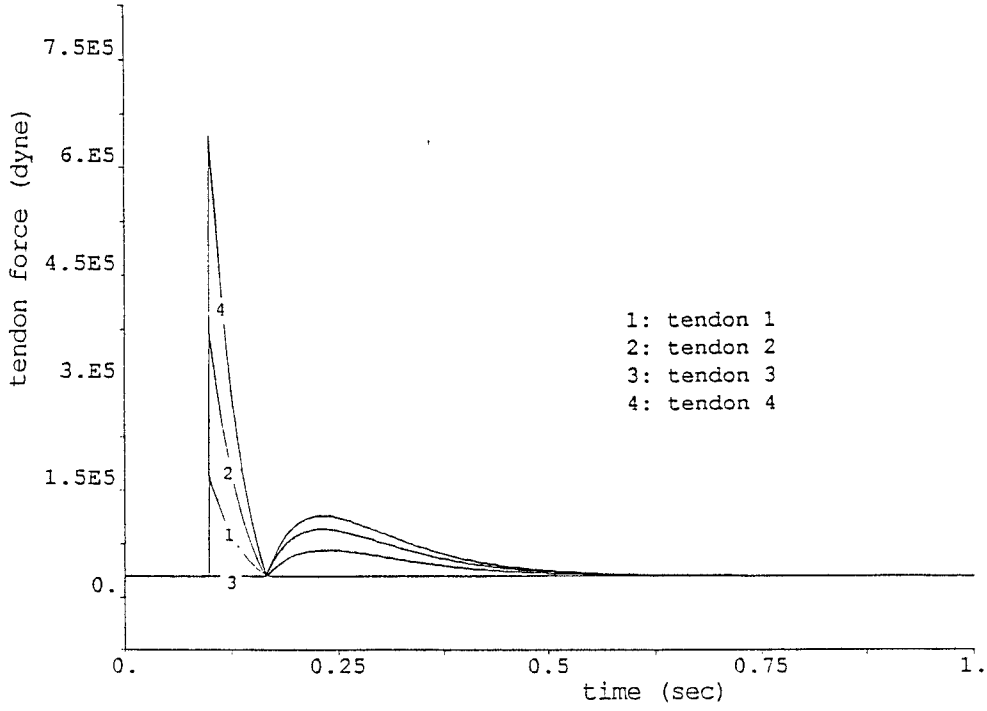

Fig. 13 Tendon force response without considering motor inertia and viscous friction (K_p=225 and K_v=30)

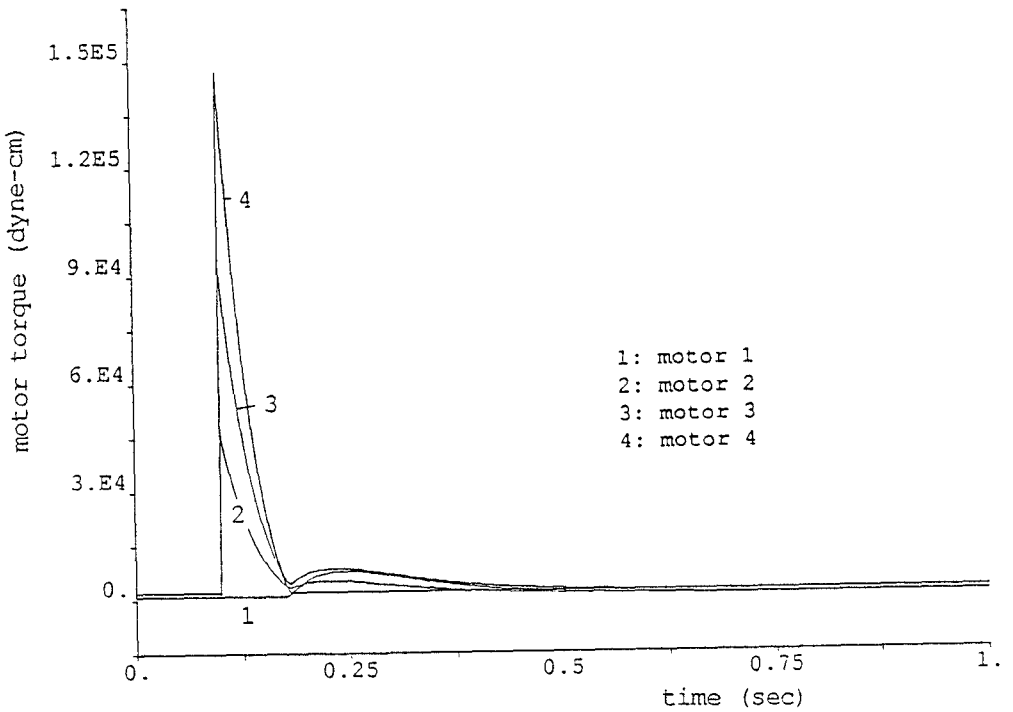

Fig. 14 Motor torque response for the structure shown in Fig. 2(a), peak value= 1.47 $\times 10^5$ dyne-cm

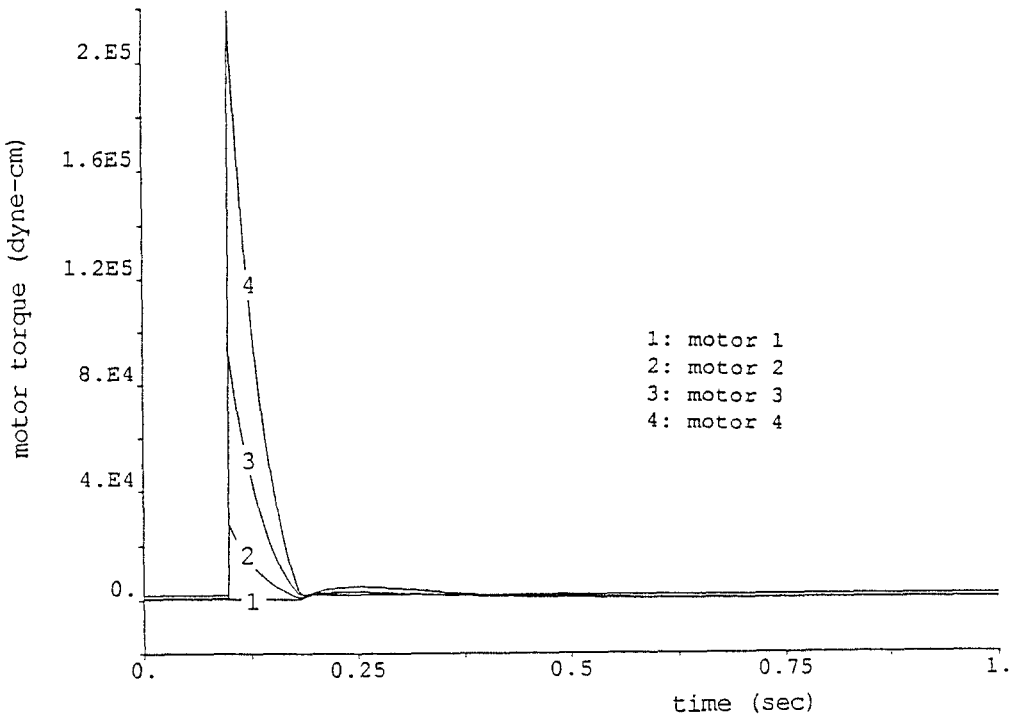

Fig. 15 Motor torque response for the structure shown in Fig. 2(b), peak value= 2.19 $\times 10^5$ dyne-cm

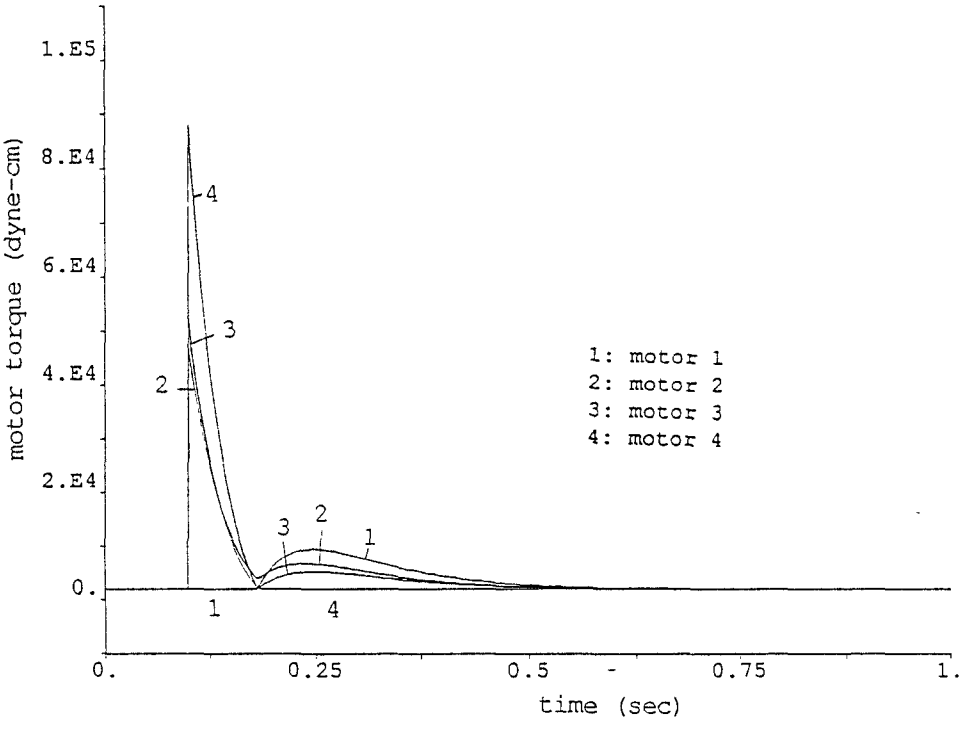

Fig. 16 Motor torque response for the structure shown in Fig. 2(c), peak value= 8.88 $\times 10^4$ dyne-cm

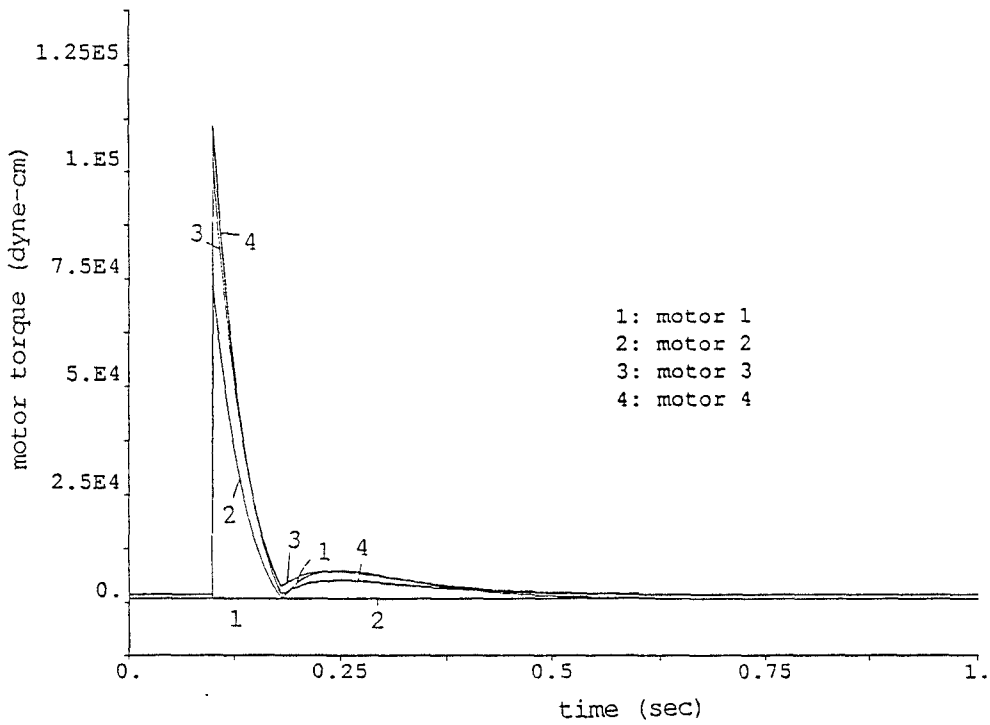

Fig. 17 Motor torque response for the structure shown in Fig. 2(e), peak value= 1.11 $\times 10^5$ dyne-cm